CO$_2$ capture by vacuum swing adsorption: role of multiple pressure equalization steps

Augustine Ntiamoah[1,2] · Jianghua Ling[1,2,3] · Penny Xiao[1,2] · Paul A. Webley[1,2] ·
Yuchun Zhai[3]

Abstract The performance of a 4-bed/16-step vacuum swing adsorption cycle containing three pressure equalization (PE) steps has been analysed in order to understand the role played by the multiple PE steps in the process performance. The cycle was designed for CO$_2$ capture from a feed gas mixture of 15 %CO$_2$/85 %N$_2$, with zeolite ×13 adsorbent from UOP (PSO2HP). Simulations were performed with the help of the commercial Aspen Adsorption simulator to help interpret the experimental results. It was found that CO$_2$ loading decreased only slightly, but N$_2$ loading decreased significantly and uniformly across the bed after each PE step. Thus, while CO$_2$ working capacity remained almost constant, working selectivity and CO$_2$ product purity increased with the number of PE steps. An experimental purity of 91.3 mol% CO$_2$ could be obtained at a recovery of 77 % at 3 kPa desorption pressure, with a cycle containing 3 pressure equalisation steps. Specific energy consumption (calculated with a constant pump efficiency of 70 %) was calculated as 0.3 MJ/kg CO$_2$, which was lower than the 1 and 2 pressure equalisation cycles. We evaluated 2-bed and 3-bed cycles containing one and two pressure equalisation steps respectively, by means of simulation in order to compare their performance with the base 4-bed 3PE cycle. For a constant recovery of 75–77 %, CO$_2$ product purities increase by 7.4 and 4.2 % (relative) in going from 1PE, to 2PE and 3PE cycles respectively, at an evacuation pressure of 3 kPa. Specific energy consumption also decreased with the number of PE steps, owing to the lowering of the starting pressure for desorption and some savings in repressurization energy with the number of PE steps. The specific energy dropped by 13 % in going from 1PE to 2PE and 3PE steps. However, the extra beds and extra cycle time required for the 3PE steps led to a reduction in productivity by almost 33 % in going from the 2PE to 3PE cycles. The choice for including additional PE steps therefore relies on the tradeoff of capital and operating costs which is strongly location and project specific.

Keywords CO$_2$ capture · Vacuum swing adsorption · Multiple pressure equalization

1 Introduction

Vacuum swing adsorption (VSA) is the most researched adsorption technique for post-combustion CO$_2$ capture, mainly because the flue gas is available at atmospheric pressure. Adsorption occurs at slightly elevated pressure but the desorption pressure is reduced to vacuum in order to obtain the needed pressure differential for desorption (Ruthven et al. 1994). Often, the goal of the separation is to recover as much of the desirable product as possible at a specified purity level. For carbon capture and sequestration (CCS), a product with >95 % CO$_2$ purity is required. High throughput and low specific energy consumption are also essential in order to enhance the process economics. Considering that the flue gas contains only about 15 % CO$_2$, achieving this high purity target in a cost-effective manner can be very challenging.

✉ Paul A. Webley
paul.webley@unimelb.edu.au

1   Cooperative Research Centre for Greenhouse Gas Technologies (CO2CRC), Melbourne, Australia

2   Department of Chemical & Biomolecular Engineering, The University of Melbourne, Parkville, VIC 3010, Australia

3   School of Material and Metallurgy, Northeastern University, Shenyang 110004, Liaoning, People's Republic of China

For the CO_2/N_2 system, CO_2 is the more strongly adsorbed by the adsorbent. However, some N_2 is also co-adsorbed and held within the void spaces between the adsorbent particles and within the pores of the adsorbent. To obtain higher product purity, it is necessary to remove as much of these gases as possible before recovering the CO_2 product. This has been mainly achieved by employing a co-current high pressure purge using previously collected CO_2 product (which is also referred to as a product rinse or heavy reflux step) prior to desorption (Chue et al. 1995; Kikkinides et al. 1993; Na et al. 2002; Reynolds et al. 2008; Takamura et al. 2001; Wang et al. 2013; Zhang and Webley 2008). During this operation, N_2 trapped in the bed void spaces or even adsorbed N_2 is flushed out or displaced by the strongly adsorbed CO_2. It has been demonstrated experimentally that higher purity can also be achieved by using co-current (or forward) blowdown, which removes more N_2 from the top of the bed (Krishnamurthy et al. 2014). A two-stage VSA process, comprising simple cycles without the heavy reflux step for each stage, can also yield higher separation efficiency (Cho et al. 2004; Shen et al. 2012). This however, is at the expense of additional capital cost.

Pressure equalization (PE) can also be used to rid the bed of void space gases to enhance the purity of the extracted CO_2 product. By PE, gas from a high-pressure bed is used to partially pressurize a low-pressure bed until their pressures equalize, thus, providing a means to internally utilize the mechanical energy contained in a high-pressure gas (Ruthven et al. 1994; Waldron and Sircar 2000; Warmuzinski 2002). During PE in the CO_2/N_2 system, the gas transferred from the high-pressure bed is mainly N_2 in the void spaces of the bed ahead of the CO_2 front, and even some co-adsorbed N_2 that is eluted from the bed as the bed pressure is reduced; thus the bed will be enriched in CO_2 before desorption (Xiao et al. 2008; Zhang and Webley 2008).

The extent of equalization is limited by the pressure gradient between the two beds; however, with more columns, more PE steps can be employed to transfer more of the void space gas to other beds. Multiple PE steps are widely practiced in commercial H_2-PSA systems where multiple adsorber columns (typically 4–10 columns) are employed for the separation (Benkmann 1989; Sircar and Golden 2000; Xu and Weist 2002). A well-known example is the "Polybed" H_2-PSA process of Union Carbide Corporation in which 3 PE steps are used (Sircar and Golden 2000; Sircar and Kratz 1988). In addition to energy savings, the multiple PE steps significantly improve the recovery of H_2 (the non-adsorbed component). Significant recovery benefits of the PE step may be generally limited to the lighter component. Therefore, the expected benefits from multiple PE steps in the VSA system for CO_2 capture

(CO_2 being the heavier component) is in the increase in CO_2 product purity rather than recovery.

This work aimed to study the role of multiple PE steps in the CO_2 VSA process. A 4-bed VSA experimental system was used, which allowed for a maximum of three PE steps in the cycle design. Simulations were also performed using the commercial Aspen adsorption simulator to help to interpret the experimental results. We did not include product rinse or heavy product purge step in the cycle, to avoid complicating the effect of multiple PE steps alone. A gas mixture with 15 %CO_2/85 %N_2 was used as feed gas, with zeolite $\times 13$ (PSO2HP-UOP) as the adsorbent. It must be noted that the study was not aimed at developing an optimal VSA cycle and determining conditions capable of achieving the high separation performance required for CCS, but rather to provide an analysis of how multiple PE steps could affect the CO_2 VSA process performance. Hence extensive variation of the operating conditions was not pursued.

2 Process description

The VSA cycle studied consists of 4 beds and 16 steps, with the step sequence illustrated in Fig. 1a for one bed, while Fig. 1b gives the operating schedule for all the four beds showing the interactions/couplings among the beds. Each bed is co-currently depressurized three times after adsorption, and the depressurization gas is used for PE with the three other beds through direct top–top bed connections. Operating three PE steps in a four-bed system however, leads to a short time interval in which feed flow is interrupted. The beds also idle during certain periods of the cycle, as they have to wait until an interaction gas becomes available. While this may not appear an attractive design, it is appropriate for the purposes of this study. Coupled adsorption and desorption steps were given much longer time while PE and repressurization steps (also coupled together) were given a fixed shorter time of 5 s. This shorter duration proved adequate for the experimental system, however, on much larger scale, a longer duration may be required for switching large industrial valves. This may affect the productivity of the cycle with more PE steps.

3 Adsorbent and bed characteristics

Zeolite NaX (commonly called $\times 13$) is the most widely used adsorbent for CO_2 capture operations because of its relatively faster kinetics, and higher working capacity and selectivity for CO_2 (Maring and Webley 2013). Zeolite $\times 13$ (PSAO2HP, manufactured by UOP) was therefore used in this study. CO_2 and N_2 isotherms on the adsorbent, fitted to dual-site Langmuir (DSL) model, have been

(a)

(b)

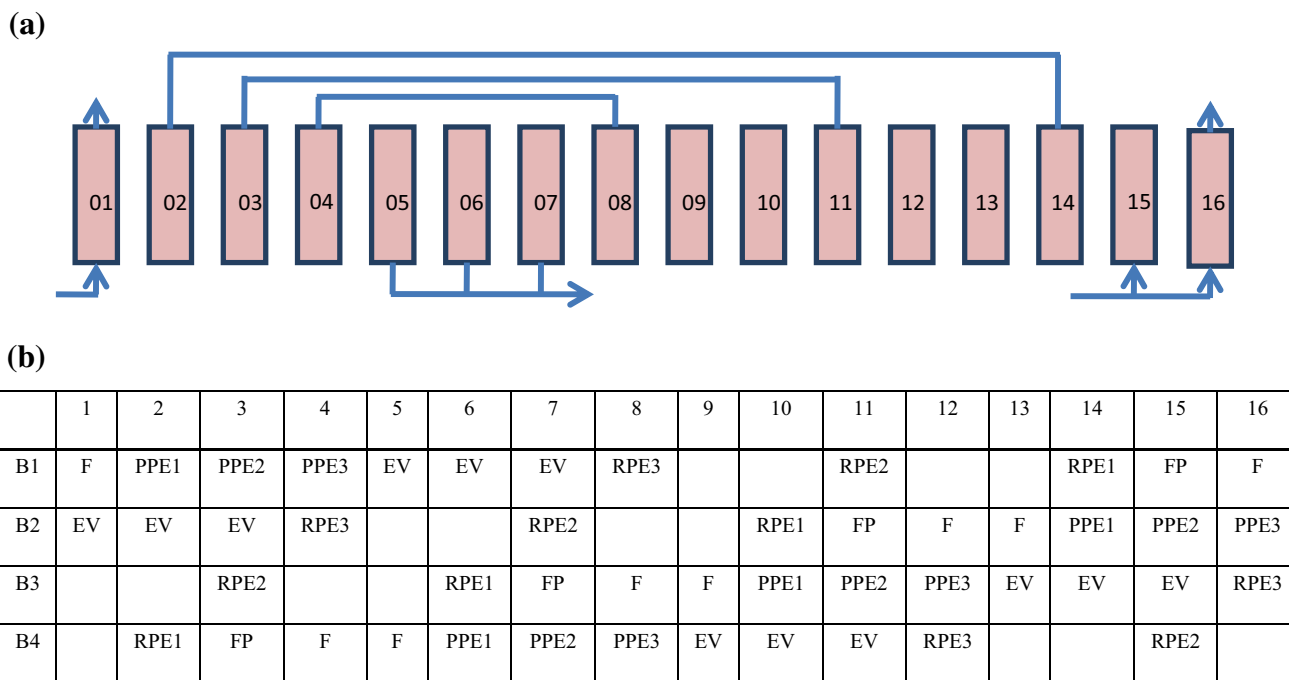|	1	2	3	4	5	6	7	8	9	10	11	12	13	14	15	16
B1	F	PPE1	PPE2	PPE3	EV	EV	EV	RPE3			RPE2			RPE1	FP	F
B2	EV	EV	EV	RPE3			RPE2		RPE1	FP	F	F	PPE1	PPE2	PPE3
B3			RPE2			RPE1	FP	F	F	PPE1	PPE2	PPE3	EV	EV	EV	RPE3
B4		RPE1	FP	F	F	PPE1	PPE2	PPE3	EV	EV	EV	RPE3			RPE2	

Fig. 1 Operating sequence for the main cycle studied. *F* feed (adsorption), *PPE* provide pressure equalization, *EV* evacuation (desorption), *RPE* receive pressure equalization, *FP* repressurization by feed gas

previously reported by our group (Xiao et al. 2008). The isotherm parameters, based on the conventional form of the model (Eq. 1), are reproduced in Table 1. The form of the isotherm equation used in Aspen Adsorption and the equivalent values of the model parameters are also provided in Eq. 2 and Table 2 respectively, for convenience. The physical properties of the adsorbent and general characteristics of the bed as used in the simulations are also listed in Table 3.

$$q_i = \frac{m_1 b_i p_i}{1 + b_i p_i} + \frac{m_2 d_i p_i}{1 + d_i p_i} \text{ with } b_i = b_{oi} \exp\left(\frac{Q_{1i}}{RT}\right)$$
$$\text{and} \quad d_i = d_{oi} \exp\left(\frac{Q_{2i}}{RT}\right) \tag{1}$$

where q_i is equilibrium loading of component i (kmol/kg-adsorbent), p_i is equilibrium partial pressure of component i (bar), m_i = saturated adsorbed phase loading in gmole/(kg ads), Q_i = heat of adsorption for component i in

J/gmole, T = temperature (K), and R = universal gas constant.

$$q_i = \frac{IP_{1i} \times \exp\left(\frac{IP_{2i}}{T}\right) \times P_i}{1 + IP_{3i} \times \exp\left(\frac{IP_{4i}}{T}\right) \times P_i} + \frac{IP_{5i} \times \exp\left(\frac{IP_{6i}}{T}\right) \times P_i}{1 + IP_{7i} \times \exp\left(\frac{IP_{8i}}{T}\right) \times P_i} \tag{2}$$

Units of the isotherm parameters are derived as IP_1 = kmol kg^{-1} bar^{-1}; IP_2 = K; IP_3 = bar^{-1}; IP_4 = K; IP_5 = kmol kg^{-1} bar^{-1}; IP_6 = K; IP_7 = bar^{-1} and $IP8$ = K.

4 Experimental equipment and operating procedure

Figure 2 shows a simplified schematic diagram of the 4-bed experimental VSA equipment used. The columns are well insulated to reduce the effect of ambient conditions on

Table 1 Dual-site Langmuir adsorption equilibrium parameters of CO_2 and N_2 on UOP PSO2HP zeolite ×13 based on Eq. 1 (Xiao et al. 2008)

Gas	m_1 (mol/kg)	b_o (1/kPa)	Q_1 (J/mol)	m_2 (mol/kg)	d_o (1/kPa)	Q_2 (J/mol)
CO_2	2.8080	4.731×10^{-7}	32194	2.4975	3.300×10^{-8}	32176
N_2	2.0197	2.036×10^{-6}	14875	0	0	0

Table 2 Dual-site Langmuir adsorption equilibrium parameters of CO_2 and N_2 on UOP PSO2HP zeolite $\times 13$ used in Aspen adsorption simulations

Component	IP(1)	IP(2)	IP(3)	IP(4)	IP(5)	IP(6)	IP(7)	IP(8)
CO_2	1.82×10^{-8}	5302.374	3.18×10^{-5}	4809.198	2.71×10^{-7}	3349.518	3.85×10^{-5}	3684.765
N_2	3.80×10^{-7}	2066.850	0.017	0	0	0.549	0.776	4.157

Table 3 Adsorbent and bed characteristics used in the Aspen adsorption simulations

Parameter	Value
Number of adsorbent beds	4
Packing length (m)	0.90
Internal bed diameter (m)	0.02
Wall thickness used (m)	0.003
Sorbent mass used per bed (kg)	0.195
Packing density (kg/m^3)	689.3
Inter-particle voidage, ε_i (m^3 void/m^3 bed)	0.35
Intra-particle voidage, ε_p (m^3 void/m^3 bead)	0.60
Pellet diameter, Dp (m)	0.002
Adsorbent shape factor (Sphericity), SFac	0.83
Adsorbent specific heat capacity, Cps (kJ/kg K)	1.0
Heat of adsorption, $\Delta H(CO_2)$ (MJ/kmol)	−35
Heat of adsorption, $\Delta H(N_2)$ (MJ/kmol)	−16

the system. The piping system is made of ¼-inch ss-tubing, plumbed with Swagelok fittings. Solenoid valves (Swage-lock SS-4BK-1D) are used to change gas flow directions. The plant is controlled via a GE Fanuc (series 90-30) PLC controller, while process monitoring and data logging are achieved with a Citect/SCADA (supervisory, control and data acquisition) system. All the valves are pneumatically operated. Switching of the solenoid valves are done automatically according to programmed PLC (programmable logic control) logic developed with a GE Fanuc Proficy Machine Edition 7.0 for automatic operation of the cycle. The plant is well instrumented to measure gas flows, gas compositions, pressures and temperatures.

During adsorption, the solenoid valves on the feed and waste lines for the bed concerned are opened, such that the feed gas stream enters the bed from the bottom for the selective adsorption of CO_2, while N_2 exits through to the waste tank. For PE, the top–top connecting valves are opened to allow gas transfer from a higher pressure bed to one at a lower pressure. Desorption is also achieved by opening the respective valve on the vacuum line to allow counter-current flow of CO_2 with the help of the vacuum pump. The beds are repressurized by first receiving gas from other columns during PE and later by receiving feed gas (with the inlet feed valve opened and all other valves

closed) to complete the repressurization process. The experimental equipment provides for the use of gas from the product tank for purge as well as gas from the waste tank for repressurization; but these were not utilized in the current study.

Experiments were performed under room temperature (20 °C). The feed pressure used is only slightly above atmospheric (105–108 kPa). Feed stream conditions (i.e. temperature, pressure, and composition) and chosen feed velocity, 0.25 ms^{-1} were all fixed. Two of the important parameters that affect both product purity and recovery are the vacuum pressure reached at the end of desorption and amount of CO_2 allowed to break through the column during adsorption, which also depends on both adsorption time and vacuum pressure. These two parameters were varied. The vacuum pressure was varied between only 3 and 5 kPa in order to limit the number of experiments. By fixing the amount of CO_2 allowed in the waste stream for a given set of runs, product recovery will be fixed; however, product purity, specific energy consumption, and productivity will all differ.

The operating conditions are summarized in Table 4.

5 Simulation in Aspen adsorption

A simulation model was developed in Aspen adsorption to match the cycle with three PE steps studied experimentally (Fig. 1). The model was further used to predict the performance of cycles with one- and two- PE steps (described later).

Aspen Adsorption solves the governing model equations for adsorption, consisting of a set of partial differential equations describing the mass, momentum and energy transport between the gas and solid phases, as well as various equilibrium isotherm models. Several specifications/assumptions were made in modelling the process in order to match the current experimental system.

5.1 Mass balance

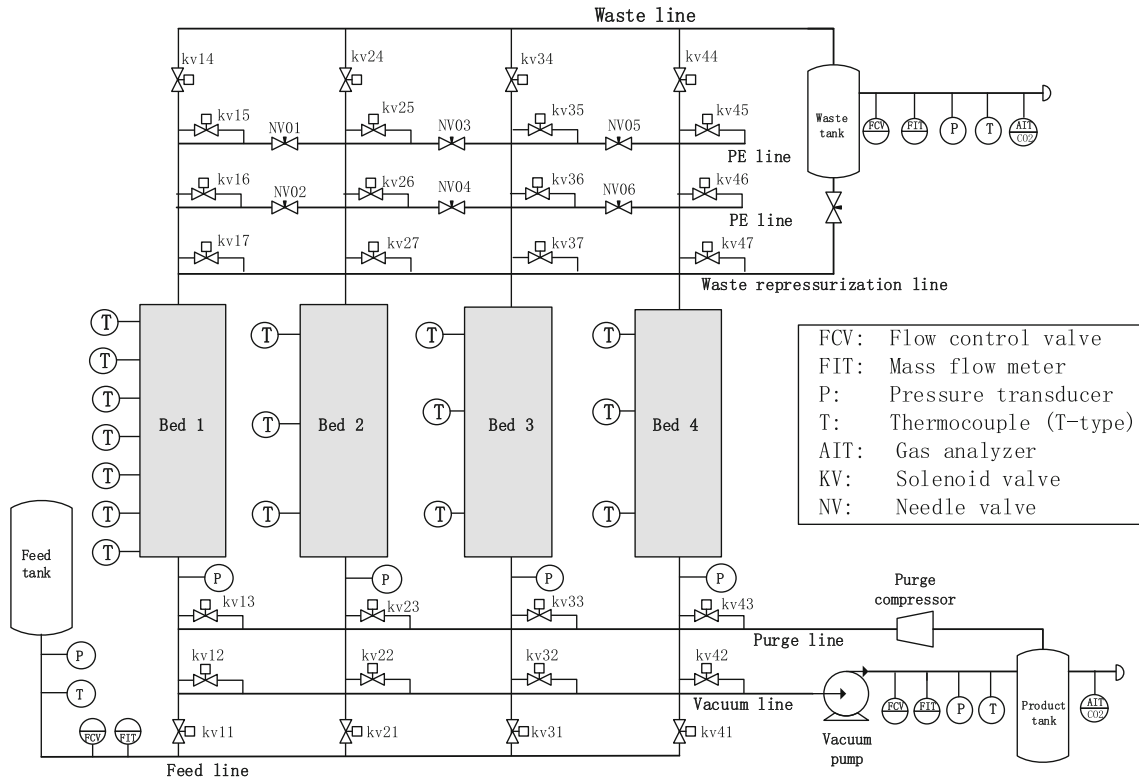The general unsteady-state mass balance over a section dz of the bed length is:

Fig. 2 Schematic diagram of the 4-bed pressure/vacuum-swing adsorption rig used

Table 4 Operating conditions for 4bed cycle with 3PE steps

Run	Ads.P (kPa)	Des.P (kPa)	Avg. flowrate (F & FP) (L/min)	Step times				
				t_{FP} (s)	$t_{F\,(total)}$ (s)	t_{PE} (s)	*$t_{EV\,(total)}$ (s)	Cycle time (s)
1	108	3.0	5.0	5	150	5	155	640
2	108	3.0	5.0	5	100	5	105	440
3	108	3.0	5.0	5	50	5	55	240
4	108	3.0	5.0	5	40	5	45	200
5	108	5.0	5.0	5	70	5	75	320
6	108	5.0	5.0	5	40	5	45	200
7	108	5.0	5.0	5	30	5	35	160

*$t_{EV(total)} = t_{F(total)} + t_{PE}$

Legend: *Ads.P* adsorption pressure, *Des.P* desorption pressure, *F* feed, *FP* feed pressurization, *PE* pressure equalization, *EV* evacuation

{Mass accumulation in gas phase}
+ {Mass adsorbed in solid phase}
+ {Mass flux by convection to bed}
− {Axial dispersion in bed}
= 0

$$\varepsilon \frac{\partial c_i}{\partial t} + \rho_b \frac{\partial q_i}{\partial t} + \frac{\partial(\upsilon_o c_i)}{\partial z} - \varepsilon_i E_z \frac{\partial^2 c_i}{\partial z^2} = 0 \qquad (3)$$

where c_i = gas-phase concentration (kmol/m^3), ε = external void fraction of the bed (or bed porosity), $\upsilon_o = $ = superficial velocity in the empty bed (m/s) ρ_b = bulk density (kg/m^3) and E = axial dispersion coefficient (m^2/s).

(i) Gas flow is 1-dimensional and axial dispersions effects are negligible. Thus, the last term on the left-hand side of Eq. 2 is neglected

(ii) P–V–T relationships for the gas stream are described by the ideal gas law.

(iii) Rate of mass transfer is described by the linear driving force model (Ruthven et al. 1994)

$$\frac{\partial q_i}{\partial t} = k_i\left(q_i^* - q_i\right) \tag{4}$$

where q_i^* is equilibrium adsorbent loading of component i (mol/kg) and k_i is mass transfer coefficient of component i (1/s).

(iv) The equilibrium relationship for the adsorbed components (q_i^*) is computed from the DSL model (see Eq. 1 above).

5.2 Momentum balance

Pressure drop through the bed is estimated by the popular Ergun equation, which is valid for both laminar and turbulent flow regimes.

$$\frac{\partial P}{\partial z} = -\left(\frac{150 \times 10^{-5}\mu_g(1-\varepsilon_i)^2}{(2r_p\psi)^2\varepsilon_i^3}\upsilon_g + \frac{1.75 \times 10^{-5}M_W\rho_g(1-\varepsilon_i)}{(2r_p\psi)\varepsilon_i^3}\upsilon_g^2\right) \tag{5}$$

where ψ is particle sphericity or shape factor, r_p is particle radius and ε_i is interparticle voidage.

5.3 Heat transfer model

The beds were considered non-isothermal (due to the appreciable swing in bed temperature observed in the experiments). Aspen Adsorption provides sets of equations to represent heat transport for non-isothermal systems. A film resistance model is used to represent the actual heat transfer between the gas and solid, which is given by:

Rate of heat transferred per unit volume
$$= HTC\, a_p(T_g - T_s) \tag{6}$$

where a_p is specific particle surface per unit volume of bed, m^2−(particle area)/m^3 (bed); and HTC is gas–solid heat transfer coefficient (MJ/m^2/K). HTC was estimated by the software using the Colburn j-factor correlation (Aspen 2011; Bird et al. 1960) (Eq. 7).

$$HTC = jC_{pg}v_g\rho_g Pr^{-2/3} \tag{7}$$

where C_{pg} is fluid phase heat capacity, J/kg/K; ρ_g is fluid-phase density, kg/m^3; v_g is fluid phase velocity, m/s and $j = 1.66Re^{-0.51}$ for Re <190, otherwise $j = 0.983Re^{-0.41}$.

The software solves the partial differential equations using the numerical method of lines. The first-order Upwind Differencing Scheme (UDS1) was selected (with 150 nodes) as the method for spatial discretization, with the

integration of the resulting ordinary differential equations performed by the Implicit Euler integrator. A simulation flowsheet based on the 'Single Bed Approach', was adopted, which simulates the behaviour of only one bed. Material to be exchanged with other beds is temporarily stored in an interaction tank, which is later returned to the bed based on a first-in-first-out principle. Dead volumes at both ends of the experimental system were estimated and taken into account in the simulations.

The multiple PE steps were handled in the simulation by specifying the pressure levels reached at the end of each equalization in the cycle organizer, which were based on the values achieved in the experiments. The criteria used to confirm attainment of cyclic steady state was when thermal and concentration profiles at the end of a cycle is within a relative tolerance value of 1×10^{-5} compared to the values of the previous cycle.

6 Results and discussion

6.1 Column breakthrough and validation of simulation model

The software could estimate the value of the mass transfer coefficient (k-value) based on the prevailing conditions in the column. However, in order to facilitate smooth running of the fairly complex problem at hand, a constant k-value was specified in the simulation flowsheet, which was obtained by fine-tuning the initial calculated value until a good match was achieved between predicted and
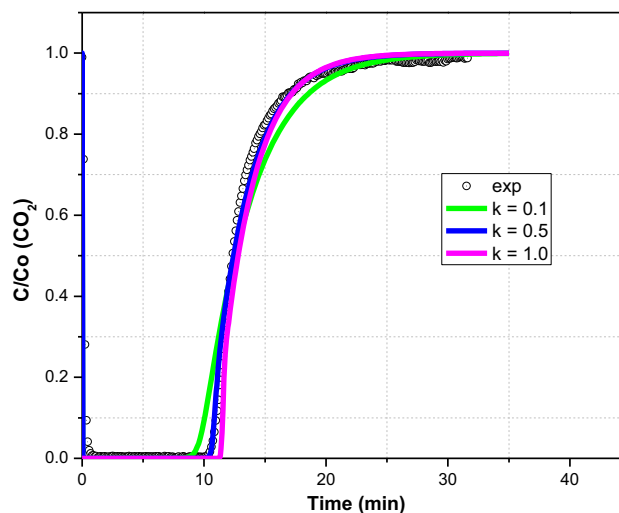

Fig. 3 Comparison of experimental and simulated breakthrough at different k-values. *Circle* = experiment, *line* = simulation (conditions: feed gas = 15 %CO_2/85 %N_2, operating pressure = 105 kPa, mass of adsorbent in column = 0.195 kg, actual feed flowrate = 5 L/min (equivalent to flow velocity of = 0.25 m/s)

experimental breakthrough curves. Figure 3 shows the breakthrough curves with the mass transfer coefficient (k-value) varied between 0.05 and 1.0 s^{-1}, based on which a value of 0.5 s^{-1} was selected. (For clarity, only three k-values are shown on the plot). This is the breakthrough curve for the feed mixture on a clean bed. The good match between predicted breakthrough and cyclic performance with the experimental results is an indication that the system studied was close to equilibrium.

6.2 Cycle performance criteria

Key performance criteria are described in Eqs. 8–10.

6.2.1 CO_2 purity (mol% CO_2)

This is the CO_2 average molar fraction in the product collected during the desorption steps.

$$CO_2 \text{ Purity} = \frac{\sum_{i=1}^{n} C_{CO2} \dot{Q}_{vac} \Delta t_i}{\sum_{i=1}^{n} \dot{Q}_{vac} \Delta t_i} \quad (8)$$

The instantaneous vacuum flow rate is measured with a mass flowmeter (Yokogawa) and the instantaneous CO_2 concentration is measured with a CO_2 composition analyser (Servomex).

6.2.2 CO_2 recovery (%CO_2)

This represents the fraction of CO_2 in the feed that is recovered during the desorption step. The main point of loss of CO_2 is through the feed effluent; hence, recovery is calculated with reference to the CO_2 lost in the waste stream.

$$\text{Recovery} = \frac{CO_2 in - CO_2 out}{CO_2 in} \quad (9)$$

6.2.3 Energy consumption (kJ)

The energy consumed is calculated by using the adiabatic power law. Since the pressures and flow rates change during the pump down and feed steps, we obtain the total energy by integrating the power law equation by multiplying the instantaneous power by the scan time in the PLC program and then summing over the total cycle time. Here we assume negligible power consumption during the relatively shorter periods the compressor and vacuum pump are idling as there are no flows through the devices. The total energy is the integral of the power consumed by the feed blower and vacuum pump, while the specific energy is

the total energy divided by the mass of CO_2 recovered as product.

$$Energy = \sum_{i=1}^{i=n} \frac{k}{k-1} \frac{\dot{Q}_{feed}(t)P_{feed}(t)}{\eta} \left[\left(\frac{P_{feed}(t)}{P_{atm}} \right)^{\frac{k-1}{k}} - 1 \right] \Delta t_i$$

$$+ \sum_{i=1}^{i=n} \frac{k}{k-1} \frac{\dot{Q}_{vac}(t)P_{vac}(t)}{\eta} \left[\left(\frac{P_{atm}}{P_{vac}(t)} \right)^{\frac{k-1}{k}} - 1 \right] \Delta t_i \quad (10)$$

In Eqs. 8–10, C_{CO2} is an instantaneous product CO_2 concentration (%CO_2), measured using a CO_2 composition analyzer, $\dot{Q}_{feed}$ and $\dot{Q}_{vac}$ represent instantaneous feed and product flow-rate (m^3/s) respectively (measured by the flowmeters attached to the feed line and the discharge line of the vacuum pump), while $CO_2 in$ and $CO_2 out$ (mol) represent total moles of CO_2 entering (feed inlet) and exiting from the system (waste outlet). The PLC program calculates the actual stream CO_2 molar flowrates from the ideal gas law, using the recorded readings of CO_2 analyzers, pressure transmitters, thermocouples and flow meters. P is pressure, Δt is time interval (s); k is the ratio of heat capacities of the gas mixture at constant pressure and at constant volume (i.e. Cp/Cv, assumed to be 1.28 for CO_2 and 1.4 for N_2), and η is compressor/pump efficiency (0.7 assumed). Specific energy consumption is a ratio of the energy to the amount of CO_2 in the product stream.

In addition to the usual inherent minor measurement errors due to some instrument precision and calibration errors, there can also be potential uncertainties in the measured flowrates and product CO_2 concentration in particular towards the end of the desorption step due to the relatively small flow of gas (as shown later in Fig. 6). A simple material balance around the experimental system for each run showed average component CO_2 balance error of 5.8 %, and overall balance error of 2.3 %. These uncertainties could affect CO_2 product purities, productivities and specific energy consumption since they were calculated based on the product amount. Recovery is less sensitive since it was calculated based on CO_2 in the waste stream.

6.3 Analysis of cycle performance (4-bed/16-step cycle)

Of particular interest to this analysis is the bed pressure profile during the cycle (example pressure profile is shown in Fig. 4a). After adsorption, the bed pressure dropped to about 80, 50 and 24 kPa for the first, second and third PE steps respectively for desorption at 3 kPa; while it reached 27 kPa after the third PE step for a 5 kPa desorption. Temperature history after cyclic steady state has been
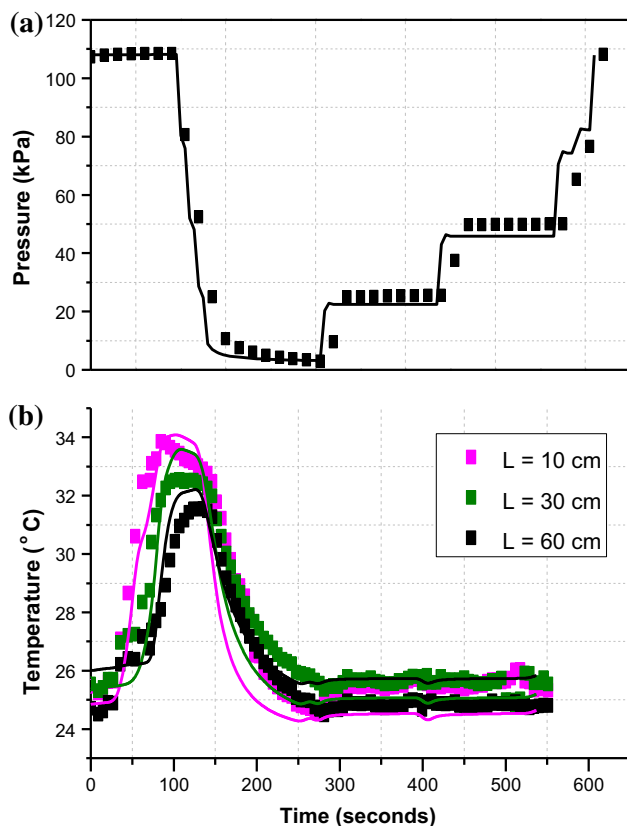
Fig. 4 Example pressure and temperature histories for a complete cycle at cyclic steady state; (Run 1, Table 5); *symbols* = experiment, *lines* = simulation

Fig. 5 Transient CO_2 composition profiles during adsorption and desorption (*symbols* are data, *lines* are simulation prediction). Squares correspond to 150 s adsorption time, *circles* correspond to 100 s adsorption time

Fig. 6 Product flowrate during desorption (evacuation) step for run 1 at CSS. *Symbol* = experiment; *Line* = simulation

reached is also shown in Fig. 4b. Even with the smaller system and relatively lower flowrate used, a temperature swing of about 8–10 °C was observed at the lower section of the bed where the majority of the adsorption and desorption occurred. Cyclic steady state was reached in all the experiments and simulations after approximately 40 cycles.

Transient CO_2 composition profiles during adsorption and desorption steps are also in shown in Fig. 5. There is significant breakthrough of CO_2 during the adsorption step for run 1 with a step time of 150 s compared with run 2 in which adsorption time is 100 s (Fig. 5a). The average CO_2 product purity is calculated by considering both the percentage composition and product flowrate (Eq. 8). As shown in Fig. 6, product flow is high initially and decreases towards the end of the desorption step.

Table 5 provides the key results of the experimental runs, showing purity, recovery, specific energy consumption and productivity at desorption pressures of 3 and 5 kPa. The experimental unit was not fitted with power meters for online reading of power consumption by the vacuum pump. Power consumption was therefore, calculated based on recorded stream flow rates and pressure ratios using a constant value of 70 % pump efficiency. The
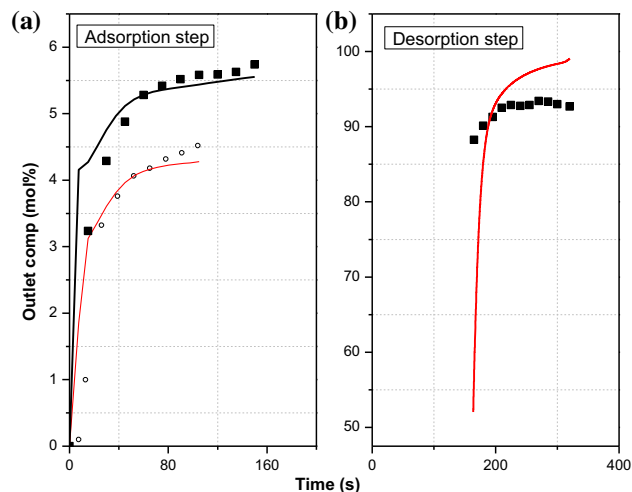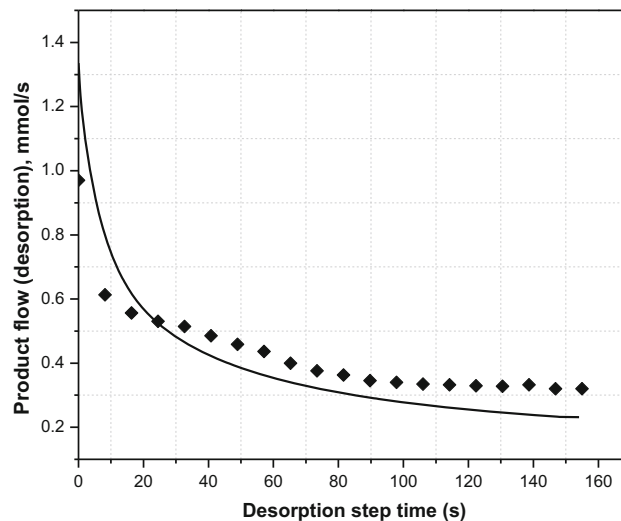
calculated energy is usually lower than the actual measured value because the pump efficiency decreases as deeper vacuum levels are reached. This was confirmed in a study by Krishnamurthy et al. (2014), who compared calculated energy with those measured using their pilot plant. Thus, the energy consumption values reported here serve only for a relative comparison between the number of PE steps and should not be compared with those from other studies on the basis of (equivalent) theoretical efficiencies.

Product purities and recoveries from experiments and simulations are also compared in Fig. 7. The different data points result from differences in adsorption step times for the various runs (as indicated in Table 4). Increase in

Table 5 Summarized process performance determined from experimental runs (4bed cycle with 3PEs)

Run	Desorption pressure	Adsorption time (s)	Recovery (mol% CO_2)	Purity (mol% CO_2)	Sp. energy (MJ/kgCO_2)	Productivity (kgCO_2/kg.ads/h)
	3 kPa					
1		150	62.9	92.4	0.28	0.067
2		100	77.0	91.3	0.26	0.088
3		50	84.5	82.5	0.23	0.085
4		40	91.3	79.5	0.23	0.093
	5 kPa					
5		70	64.5	86.5	0.25	0.072
6		40	83.7	78.8	0.22	0.062
7		30	91.3	70.5	0.30	0.043

Adsorbent = zeolites ×13 (PSO2HP-UOP), Feed gas = 15 %CO_2/85 %N_2, Adsorption pressure = 105–108 kPa, mass of adsorbent per column = 0.195 kg (=0.78 kg for 4 columns), feed velocity = 0.25 m/s. (Energy consumption was calculated using η = 70 %)
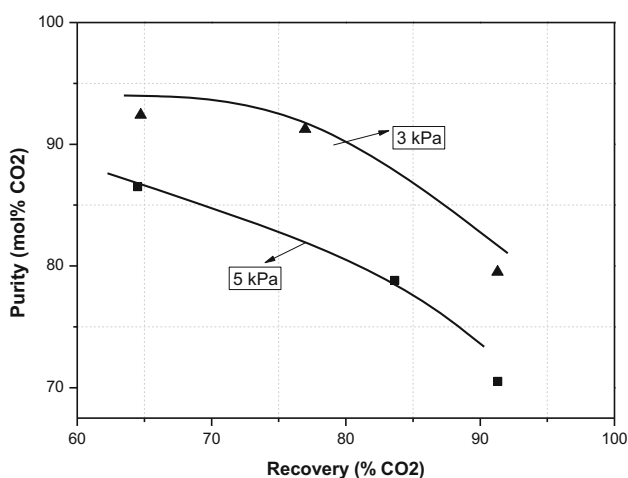

Fig. 7 Trade-off of purity and recovery for 4bed cycle with 3PE steps at 3- and 5-kPa desorption pressures: Comparison of experimental and predicted results. (*symbols* = experiment; *line* = simulation)

adsorption time also increased evacuation time by the same margin as the steps are coupled (Fig. 1b). To achieve higher recoveries, the adsorption time is shortened such that significant breakthrough of CO_2 is avoided. This means the bed is not fully utilized and less CO_2 will be adsorbed, leading to lower product purities at higher recoveries. This explains the purity-recovery trade-off shown in Fig. 7. The simulations yielded slightly higher recoveries, while purities matched very well with the experimental results. It can be seen in Fig. 4a that the simulated pressure profile during desorption is steeper than that measured, which could be due to valve coefficient settings used in the simulations; this can partly contribute to the slightly higher recoveries obtained in the simulations.

As expected, both recovery and purity values were higher for desorption at 3 kPa compared to desorption at 5 kPa. The two performance variables depend strongly on the adsorbent working capacity, which generally increases as deeper vacuum levels are reached. This can be explained by comparing loading profiles at the ends of adsorption and desorption (Fig. 8a, b) for the two desorption pressures. The amount of CO_2 recovered is proportional to the area enclosed by the two curves. At 5 kPa desorption pressure, a significant amount of the adsorbed components are not recovered (as indicated by the relatively smaller area). The bed will be comparatively not well cleaned at the end of desorption for 5 kPa, hence for the same adsorption time, more CO_2 will be lost in the high pressure adsorption step, resulting in lower recovery. On the other hand, a shorter time will be required to reach the same CO_2 front during adsorption. Hence, although less product will be collected, productivity can be higher or lower depending on whether the amount of CO_2 recovered or the shorter cycle time is the dominating factor (as shown in Table 5).

A feed time of 150 s (run 1) yielded only a slightly higher purity but much lower recovery compared with feeding time of 100 s (run 2) due to loss of more CO_2 in the feed effluent in the former case (see Fig. 5). The performance of run 2 is therefore considered better and selected for detailed analyses in the succeeding sections.

6.4 Role of pressure equalization steps

Figure 9 shows the concentration profiles within the bed at the end of adsorption and the various provide PE steps. For this particular run (run 2), feeding was continued until CO_2 breakthrough reached about 4 % of the amount in the feed; by this time the CO_2 mass transfer zone has penetrated about 60 % of the column length. Gas at the top of the column (from z/L = 0.6 to z/L = 1) is enriched in N_2. By transferring this gas in stages to other beds for PE, CO_2-mol fraction in the gas phase increases, with the lower
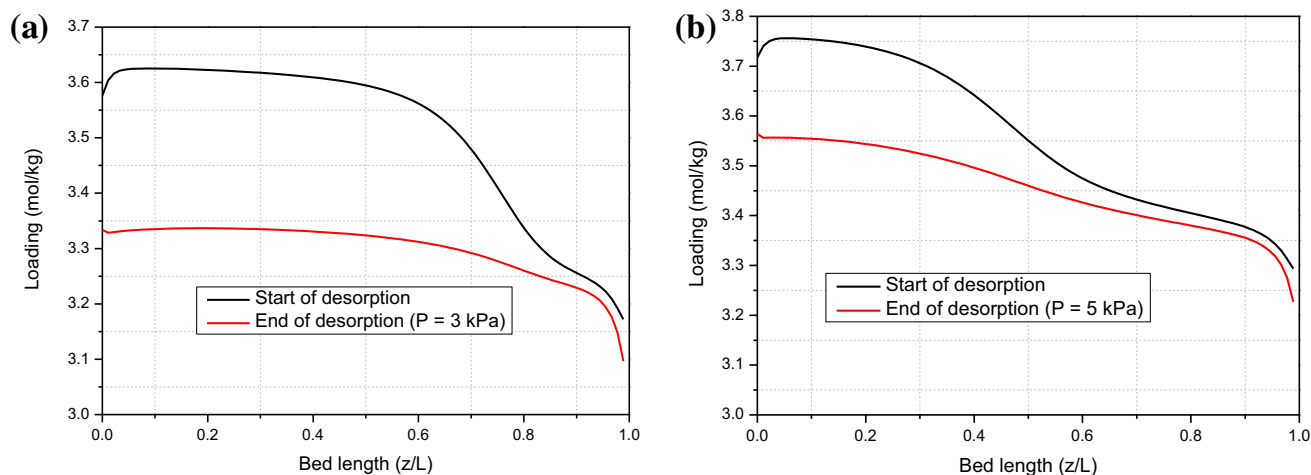
Fig. 8 Simulated axial CO_2 loading profiles at the start and end of desorption steps for different vacuum pressure levels at cyclic steady state. (The same CO_2 front in the column was maintained during adsorption). **a** = Desorption at 3 kPa, **b** = desorption at 5 kPa vacuum pressure
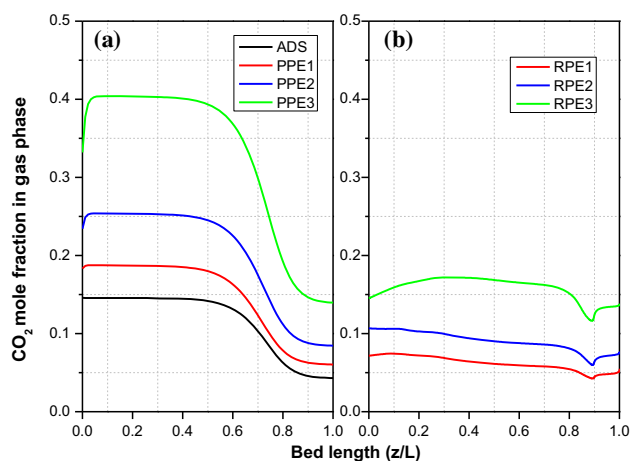

Fig. 9 Simulated steady state axial composition profiles of CO_2 inside the column at the end of selected cycle steps. Position at 0 m represents the *bottom* of the bed and flow direction is from *bottom* to the *top* of the bed. **a** provide PE; **b** receive PE

section of the bed rising from 15 % to about 40 % of the entire gas phase concentration by the end of the third PE step (Fig. 9a). The opposite behaviour occurs in the bed receiving the PE gas. After desorption, gas with more N_2 is introduced to the bed during the first receive pressure equalization step (RPE1). Subsequent equalization gas may contain a small amount of CO_2 and this minimally raises the CO_2 concentration front during the subsequent RPE steps. CO_2 mol fractions within the top of the bed packing differ slightly for the providing and receiving beds during PE due to differences in the original states of the beds even though column pressures are equalized (see concentration fronts corresponding to z/L = 0.9 in Fig. 9). The concentration profiles can be influenced by the bed void volume associated with the extra piping beyond the bed packing.

Since the void volume around the experimental system was specified in the void tanks used in the simulation flowsheet, we show the concentration within the void tanks for the bed providing and receiving equalization gas as extensions in Fig. 9 (from z/L = 0.9 to z/L = 1). It can be seen that there is a good match in mole fractions within the void volume above the packing. Thus, some of the gas exchanged is trapped within the void space. Larger void spaces (particularly in the bottom part of the bed) can store gas from the preceding steps in the line and this can have significant effect on the process performance, especially product purity. Simulation of run 2 (see Table 5) without top- and bottom- void spaces yielded a product purity of 95.3 % against a simulated value of 93.4 % for the system with void space taken into consideration. It is expected that on a larger scale where the ratio of void to actual system volume is usually low, further gain in cycle performance may be obtained.

Figure 10a, b show the loading profile (solid phase concentration) of both CO_2 and N_2 at some selected steps of the cycle. CO_2 loading is only slightly reduced due to the release of small amounts of adsorbed CO_2 into the gas phase as pressure is lowered during the PE steps. However, significant reduction in N_2 loading occurs uniformly throughout the bed with each additional PE step (Fig. 10b). Thus, while CO_2 working capacity remains almost constant, working selectivity increases with the number of PE steps. This is definitely resulting in improved purity of the extracted CO_2 product. The working capacity is considered here as the difference between the amount of CO_2 adsorbed at the end of a given PE step and the amount that remains on the bed after desorption. The working selectivity on the other hand, is the ratio of CO_2 and N_2 loadings at the ends of the given PE and desorption steps.
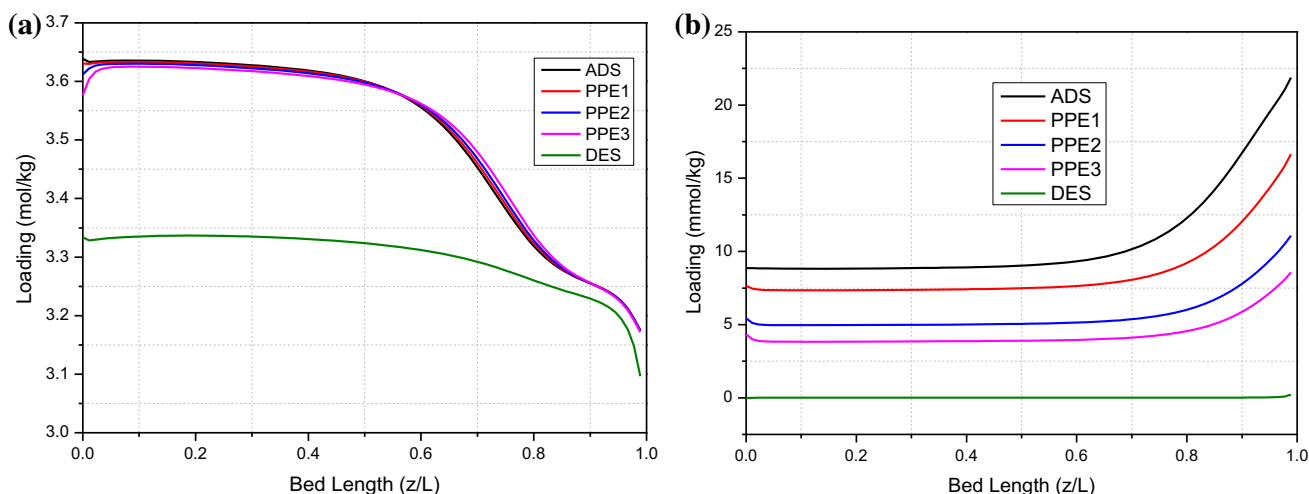
Fig. 10 Simulated axial loading profiles at the end of pressure equalization and desorption steps at cyclic steady state for vacuum pressure of 3 kPa. **a** = CO_2 loadings **b** = N_2 loadings

The adsorbent productivity relates to the cyclic working capacity as defined above, while product purity is also a function of the working selectivity, also referred to as the separation factor (SF) (Ackley 2003). Table 6 shows the working capacities and selectivities calculated from loadings at the ends of the various PE steps and the desorption step. Also shown in the last column of the table are theoretical product purities calculated by assuming that desorption was carried out at the ends of adsorption and each of the PE steps. Product purity increases with the number of PE steps which agrees with the trend in working selectivity, but the gain in purity decreases for each additional PE step. There is also a slight decrease in delta loading (or the amount of CO_2 recovered in a cycle) with increasing number of PE steps which also agrees with Fig. 10a. This is because the amount of gas in the column to be recovered reduces with the number of PE steps.

6.5 Performance comparison for cycles with 1PE, 2PE and 3PE steps

2-bed/6-step and 3-bed/9-step cycles consisting of one- and two- PE steps respectively (Fig. 11) were also simulated. The performances of these cycles are compared with the base cycle studied (i.e. 4-bed/16-step with 3PEs) in Fig. 12a–c for a desorption pressure of 3 kPa.

The specific energy consumption and productivity data plotted in Fig. 12a, c were obtained at comparable recoveries of 75–77 %, under which conditions purity were also 93.4, 89.6 and 83.3 mol% CO_2 for the cycles containing 3PE, 2PE and 1PE respectively. With recovery based on the amount of CO_2 that is lost in the effluent, recovery could be fixed by allowing the same amount of CO_2 to break through the column during the adsorption step. (The differences in amount of feed gas used for re-pressurization among the different cycle designs are ignored here because it is quite small compared with feed gas flow). As already mentioned, the energy consumption of the blower and vacuum pump were calculated; emphasis must therefore, be placed on the relative performance of the different cycles in terms of their energy consumption, rather than on the absolute energy numbers.

At a given recovery, product purity increased with the number of PE steps (Fig. 12a). The adsorption step time was varied (which also changed the desorption step time) to obtain the different data points in the graph as has been explained earlier. Under the operating conditions used, very high product purities and recoveries could not be achieved in the present cycle – indeed this was not the purpose of this study. CO_2 product purity depends on the amount of N_2 on the bed prior to desorption. In a recent study by Krishnamurthy et al. (2014), employing a

Table 6 Working capacity and selectivity at the ends adsorption and PE steps estimated by simulation (for a desorption pressure of 3 kPa)

Start of desorption	ΔqCO_2 (mol/kg.ads)	ΔqN_2 (mol/kg.ads)	$\Delta qCO_2/\Delta qN_2$	(yCO_2)-avg	(yN_2)-avg	Purity (%CO_2)
End of ADS	0.262	1.04×10^{-2}	25.22	0.132	0.857	74.1
End of PE1	0.261	7.42×10^{-3}	35.23	0.16	0.829	85.4
End of PE2	0.260	5.10×10^{-3}	51.15	0.219	0.77	90.9
End of PE3	0.260	4.09×10^{-3}	63.74	0.347	0.642	93.4

(a)

Step	1	2	3	4	5	6
Bed1	F	PPE	EV	EV	RPE	FP
Bed2	EV	RPE	FP	F	PPE	EV
Time (s)	100	5	5	100	5	5

(b)

Step	1	2	3	4	5	6	7	8	9
Bed1	F	PPE	PPE	EV	EV	RPE	ID	RPE	FP
Bed2	EV	EV	RPE	ID	RPE	FP	F	PPE	PPE
Bed3	ID	RPE	FP	F	PPE	PPE	EV	EV	RPE
Time (s)	100	5	5	100	5	5	100	5	5

Fig. 11 Schematic diagram and sequence of cycle steps in the operation of **a** 2-bed/6-step; **b** 3-bed/9-step VSA cycle for CO_2 capture

forward blowdown step, an optimal intermediate pressure of 5.6 kPa and final evacuation pressure of 2 kPa, together with adsorption pressure of 150 kPa were used to achieve high purity-recovery trade-off values of 94.8 and 89.7 % CO_2. This performance was realized without a loss in productivity; however, the extra pump which is used to aid the forward blowdown step in the VSA process may add to the operating cost. Reported calculated specific energy at comparable pump efficiency of 72 % was about 191.5 kWh/ton CO_2 (0.7 MJ/kg CO_2). In another parametric study by Haghpanah et al. (2013), also employing a forward blowdown without PE and CO_2 product rinse steps, optimal intermediate and final evacuation pressures of 16 and 3 kPa were used to achieve both high purity and recovery of 90 % CO_2. The forward blowdown step functions similarly to the PE step- to remove gas from the top of the bed and also to reduce starting pressure for the evacuation step. It is clear that by relying on this approach alone, much lower intermediate pressure than the level reached at the end of the third PE step in the current study (24 kPa) may be required to remove more N_2 gas from the top of the bed to achieve high product purity. In this way, significant loss of CO_2 through the feed step can be avoided to improve on the recovery.

Figure 12b shows the overall specific energy consumption as well as the contributions made by the feed and desorption stages to the energy consumption. The energy due to the feed step constitutes the repressurization and actual feed steps; with feeding carried out at a fixed pressure, the difference in compressor/blower energy is due to the repressurization step. The desorption by vacuum stage accounts for a significant portion of the overall specific energy consumption: 0.15 MJ/kg representing 69 % of the energy consumed by the 3PE cycle to 0.23 MJ/kg representing 74 % of the energy consumed by the 2Bed cycle with 1PE step. Consequently, there is much more savings in desorption energy with increase in the number of PE steps than savings in repressurization energy. By lowering the starting pressure for evacuation after each PE step with the final evacuation pressure fixed, there will be relatively less work to be performed by the vacuum pump. It can be seen that the margin of gain in CO_2 product purity and savings in total specific energy consumption are both smaller between 2PE and 3PE compared to the gain realized in moving from 1PE to 2PE steps (Fig. 11a, b).

The productivity is also an important performance criterion in particular for applications like CO_2 capture from flue gas where high investment cost can be an issue of concern given the high volume of feed gas flow. We
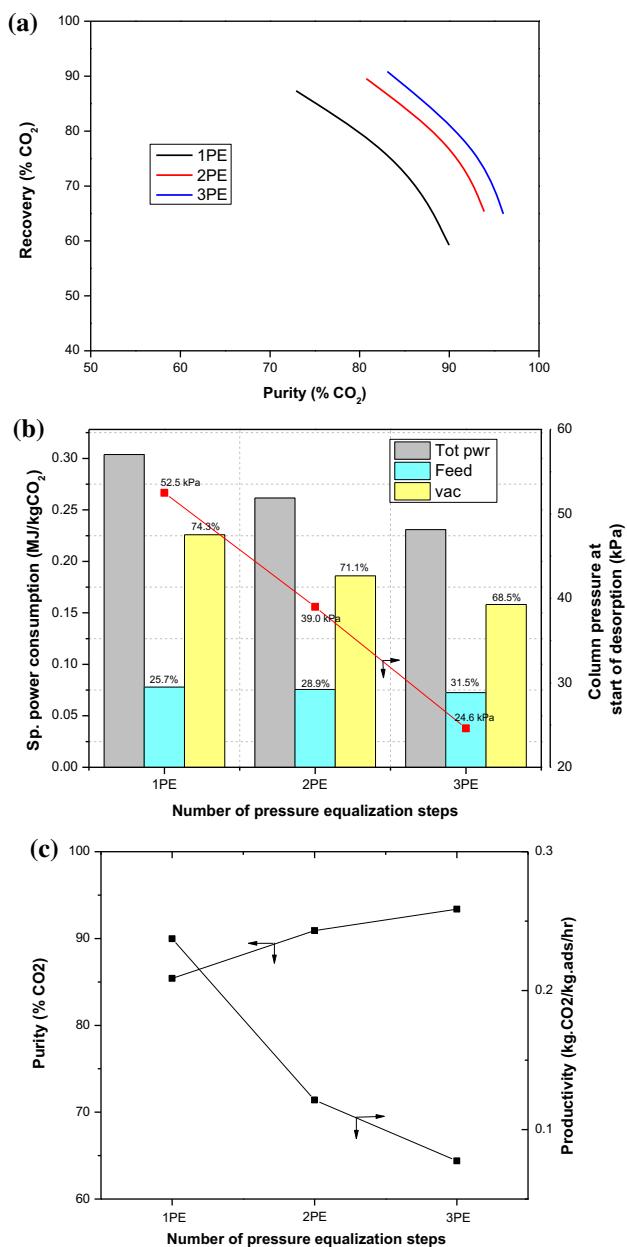
Fig. 12 Effect of increasing number of pressure equalization (PE) steps on CO_2VSA process performance. Simulated results at a desorption pressure of 3 kPa. **a** Effects of PE on CO_2 product purity. **b** Effects of PE on calculated specific energy consumption. **c** Effects of PE on system productivity

therefore show how the multiple PE steps perform in terms of adsorbent productivity in Fig. 12c. It is clear that productivity decreases by a wider margin compared to the increase in product purity with increase in the number of PE steps. This is perhaps a major drawback in the application of multiple PE steps in the CO_2 VSA process. The drop in productivity arises largely from the extra beds and extra cycle time needed to conduct the 2PE and 3PE step cycles.

Because the starting (feed) pressure is not high enough, the gains in multiple PEs may not be high enough; and it may not be deemed worthwhile to employ more adsorber columns in order to include more PE steps in the CO_2 VSA cycle. One of the likely future needs of CO_2 capture processes will be the continuous treatment of the flue gas which is emitted continuously from the power plant. This would necessitate the use of multiple adsorbent beds or two or three parallel units of the currently reported simple processes, thereby increasing the system capital cost. When multiple beds are already available, the need to include PE(s) as intermediate process steps to help reduce operating costs and enhance CO_2 product purity could become increasingly important.

7 Conclusion

The effect of the number of PE steps on the CO_2 VSA performance has been evaluated at desorption pressures of 3 and 5 kPa using both experiments and simulations. It has been shown that with more PE steps, more of the void space gas is recovered which was indicated by a large decrease in N_2 loading before desorption. This in turn, increased CO_2 working selectivity and hence, product purity. Specific power consumption also decreased as the starting pressure for evacuation was lowered with increasing PE steps.

The margin of gain in purity and savings in energy however, decreased for each additional PE step. Productivity also decreased with the number of PE steps. Therefore, the decision to employ more PE steps in the CO2VSA cycle must consider the additional resources required to accommodate each additional PE step. Savings in energy requirement must be assessed against additional capital cost required for additional PE steps. This CAPEX/OPEX tradeoff is location and project specific.

References

Ackley, M.: Application of natural zeolites in the purification and separation of gases. Microporous Mesoporous Mater. **61**, 25–42 (2003)

Aspen, 2011. Aspen adsorption v8.0 user help file. Aspen Technologies, Inc. (WWW Document)

Benkmann, C.: Six adsorber pressure swing adsorption process. US Patent 4,834,780 (1989)

Bird, R.B., Stewart, W.E., Lightfoot, E.N.: Transport Phenomena. Wiley, New York (1960)

Cho, S.-H., Park, J.-H., Beum, H.-T., Han, S.-S., Kim, J.-N.: A 2-stage psa process for the recovery of co2 from flue gas and its

power consumption. In: Sang-Eon Park, J.-S.C., Kyu-Wan, L. (eds.) Studies in Surface Science and Catalysis, pp. 405–410. Elsevier, Amsterdam (2004)

Chue, K.T., Kim, J.N., Yoo, Y.J., Cho, S.H., Yang, R.T.: Comparison of activated carbon and zeolite $\times$13 for CO2 recovery from flue gas by pressure swing adsorption. Ind. Eng. Chem. Res. **34**, 591–598 (1995)

Haghpanah, R., Nilam, R., Rajendran, A., Farooq, S., Karimi, I.A.: Cycle synthesis and optimization of a VSA process for postcombustion CO2 capture. AIChE J. **59**, 4735–4748 (2013)

Kikkinides, E.S., Yang, R.T., Cho, S.H.: Concentration and recovery of CO2 from flue gas by pressure swing adsorption. Ind. Eng. Chem. Res. **32**, 2714–2720 (1993)

Krishnamurthy, S., Rao, V.R., Guntuka, S., Sharratt, P., Haghpanah, R., Rajendran, A., Amanullah, M., Karimi, I.A., Farooq, S.: CO2 capture from dry flue gas by vacuum swing adsorption: a pilot plant study. AIChE J. **60**, 1830–1842 (2014)

Maring, B.J., Webley, P.A.: A new simplified pressure/vacuum swing adsorption model for rapid adsorbent screening for CO2 capture applications. Int. J. Greenh. Gas Control **15**, 16–31 (2013)

Na, B.K., Lee, H., Koo, K.K., Song, H.K.: Effect of rinse and recycle methods on the pressure swing adsorption process to recover CO2 from power plant flue gas using activated carbon. Ind. Eng. Chem. Res. **41**, 5498–5503 (2002)

Reynolds, S.P., Mehrotra, A., Ebner, A.D., Ritter, J.A.: Heavy reflux PSA cycles for CO2 recovery from flue gas: Part I. Performance evaluation. Adsorption **14**, 399–413 (2008)

Ruthven, D.M., Farooq, S., Knaebel, K.S.: Pressure Swing Adsorption. VCH Publishers Inc., New York (1994)

Shen, C.Z., Liu, Z., Li, P., Yu, J.G.: Two-stage VPSA process for CO2 Capture from flue gas using activated carbon beads. Ind. Eng. Chem. Res. **51**, 5011–5021 (2012)

Sircar, S., Golden, T.C.: Purification of hydrogen by pressure swing adsorption. Sep. Sci. Technol. **35**, 667–687 (2000)

Sircar, S., Kratz, W.C.: Simultaneous production of hydrogen and carbon dioxide from steam reformer off-gas by pressure swing adsorption. Sep. Sci. Technol. **23**, 2397–2415 (1988)

Takamura, Y., Narita, S., Aoki, J., Hironaka, S., Uchida, S.: Evaluation of dual-bed pressure swing adsorption for CO2 recovery from boiler exhaust gas. Sep. Purif. Technol. **24**, 519–528 (2001)

Waldron, W.E., Sircar, S.: Parametric study of a pressure swing adsorption process. Adsorption **6**, 179–188 (2000)

Wang, L., Yang, Y., Shen, W., Kong, X., Li, P., Yu, J., Rodrigues, A.E.: Experimental evaluation of adsorption technology for CO2 capture from flue gas in an existing coal-fired power plant. Chem. Eng. Sci. **101**, 615–619 (2013)

Warmuzinski, K.: Effect of pressure equalization on power requirements in PSA systems. Chem. Eng. Sci. **57**, 1475–1478 (2002)

Xiao, P., Zhang, J., Webley, P., Li, G., Singh, R., Todd, R.: Capture of CO2 from flue gas streams with zeolite $\times$13 by vacuum-pressure swing adsorption. Adsorption **14**, 575–582 (2008)

Xu, J., Weist, E.L.: Six bed pressure swing adsorption process with four steps of pressure equalization. US6454838B1 (2002)

Zhang, J., Webley, P.A.: Cycle development and design for CO2 capture from flue gas by vacuum swing adsorption. Environ. Sci. Technol. **42**, 563–569 (2008)